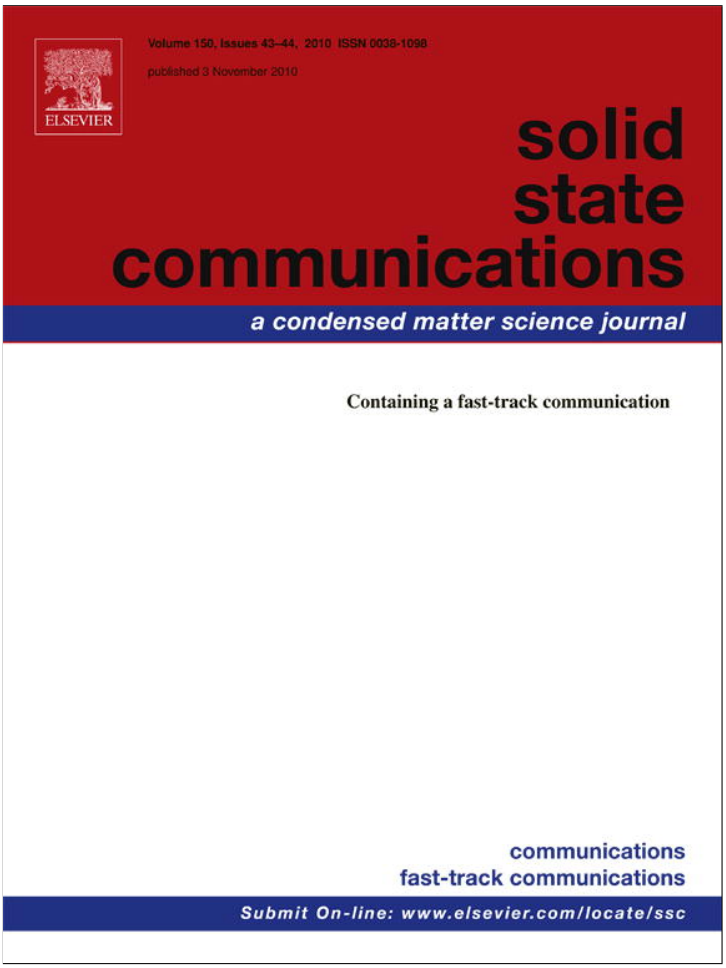

Solid State Communications 150 (2010) 2114–2117

Contents lists available at ScienceDirect

Solid State Communications

journal homepage: www.elsevier.com/locate/ssc

Mechanisms for the enhancement of the lateral photovoltage in perovskite heterostructures

Chen Ge, Kui-juan Jin *, Hui-bin Lu, Cong Wang, Guang-ming Zhao, Li-li Zhang, Guo-zhen Yang

Beijing National Laboratory for Condensed Matter Physics, Institute of Physics, Chinese Academy of Sciences, Beijing 100190, China

ARTICLE INFO

Article history:
Received 10 August 2010
Received in revised form
8 September 2010
Accepted 10 September 2010
by E.L. Ivchenko
Available online 17 September 2010

Keywords:
A. Heterostructure
D. Photovoltaics

ABSTRACT

The mechanisms for the greatly enhanced lateral photovoltaic effect in the perovskite oxide heterostructures are studied by solving *time-dependent* two-dimensional drift-diffusion equations self-consistently. By our calculations, we find that the lateral photovoltage of *p*-type material is larger than that of *n*-type material owing to the larger drift electric field induced in the *p*-type material than that in the *n*-type material. Moreover, the built-in electric field at the interface between the thin film and substrate can also enhance the lateral photovoltage. The above two mechanisms can well explain one-order-of-magnitude enhancement of the lateral photovoltaic effect in the perovskite heterostructures. In addition, we find that the materials with larger mobility ratio have a stronger Dember effect. Such an understanding of the mechanisms for the enhancement of lateral photovoltage in oxide heterostructures should be useful in further designing of the structures of position-sensitive detectors and new THz sources.

The lateral photovoltage (LPV), which was discovered by Schottky in 1930 [1] and Wallmark [2] in 1956, has been widely investigated due to its various applications. For instance, position-sensitive detectors (PSD) based on LPV are applied in many fields requiring precision measurements, such as medical instrumentation, robotic vision, and remote optical alignment, etc [3]. Recently, an unusual transient LPV phenomenon proposed as an evidence of the Dember effect in perovskite oxide heterostructures has been reported [4–6]. It is well known that the optical generation of THz radiation can be produced in the conventional semiconductors using the photo-Dember effect under ultra-short pulse laser illumination [7–10]. In the heterostructures of both $La_{0.7}Sr_{0.3}MnO_3$/Si (LSMO3/Si) and $La_{0.9}Sr_{0.1}MnO_3$/$SrNb_{0.01}Ti_{0.99}O_3$ (LSMO1/SNTO), the most significant phenomenon is that a one-order-of-magnitude enhancement of the Dember-effect-induced LPV was observed, as compared with those of the substrates [4,5]. Therefore, the understanding of the underlying physical mechanisms for such a phenomenon is fundamentally important and should be of great value for the further designing of the structures of potential applications in both high-sensitive PSDs and powerful THz sources.

In this letter, we present two physical origins for such an enhancement of LPV in the oxide heterostructures compared to that of the substrates, by solving the *time-dependent* two-dimensional drift-diffusion equations self-consistently. The theoretical results are in good agreement with the experimental data. We find that the LPV of *p*-type material is larger than that of *n*-type material, owing to the larger drift electric field induced in *p*-type material than that in the *n*-type material. Moreover, the built-in electric field at the interface between the thin film and substrate can also enhance the LPV. By calculations, we find that the materials with a large mobility ratio can be utilized for performance improvement of the devices based on the Dember effect.

LSMO1/SNTO and LSMO3/Si heterostructures were fabricated by growing a *p*-type LSMO1 (LSMO3) layer on a *n*-type SNTO (Si) substrate, with the computer-controlled laser MBE technique, following the procedure we reported previously [11]. In our experiments published elsewhere [4,5], a small area of 0.5 mm diameter was irradiated on the sample surfaces by a 308 nm XeCl excimer laser beam (the pulse width of 20 ns, the pulse energy of 0.15 mJ, and the repetition rate of one pulse every 5 min to avoid the heating effect). We moved the samples in the lateral direction and recorded the LPV values, with a sampling oscilloscope of 500 MHz terminated into 1 MΩ at ambient temperature. The schematic setup for LPV measurement is shown in the inset of Fig. 1. Fig. 1(a) [4,5] exhibits the experimental LPVs of LSMO side in the LSMO1/SNTO (the green circular curve) and LSMO3/Si (the blue square curve) heterostructures. Fig. 1(b) [4] depicts the experimental LPVs of SNTO (the green circular curve) and Si (the blue square curve) substrates. Here, the photovoltage, which denotes the peak value of the LPV between the indium electrodes A ($x = -3$ mm) and B ($x = 3$ mm) on the LSMO1 surface, depends on the laser spot position in the LSMO1/SNTO heterostructure. The diameter of indium electrodes is about 1 mm. More details of the experiments can be easily found in our previous report [5]. From Fig. 1(a) and (b), it can be seen that a one-order-of-magnitude

* Corresponding author. Tel.: +86 10 82648099.
E-mail address: kjjin@aphy.iphy.ac.cn (K.-j. Jin).

0038-1098/$ – see front matter © 2010 Elsevier Ltd. All rights reserved.
doi:10.1016/j.ssc.2010.09.016

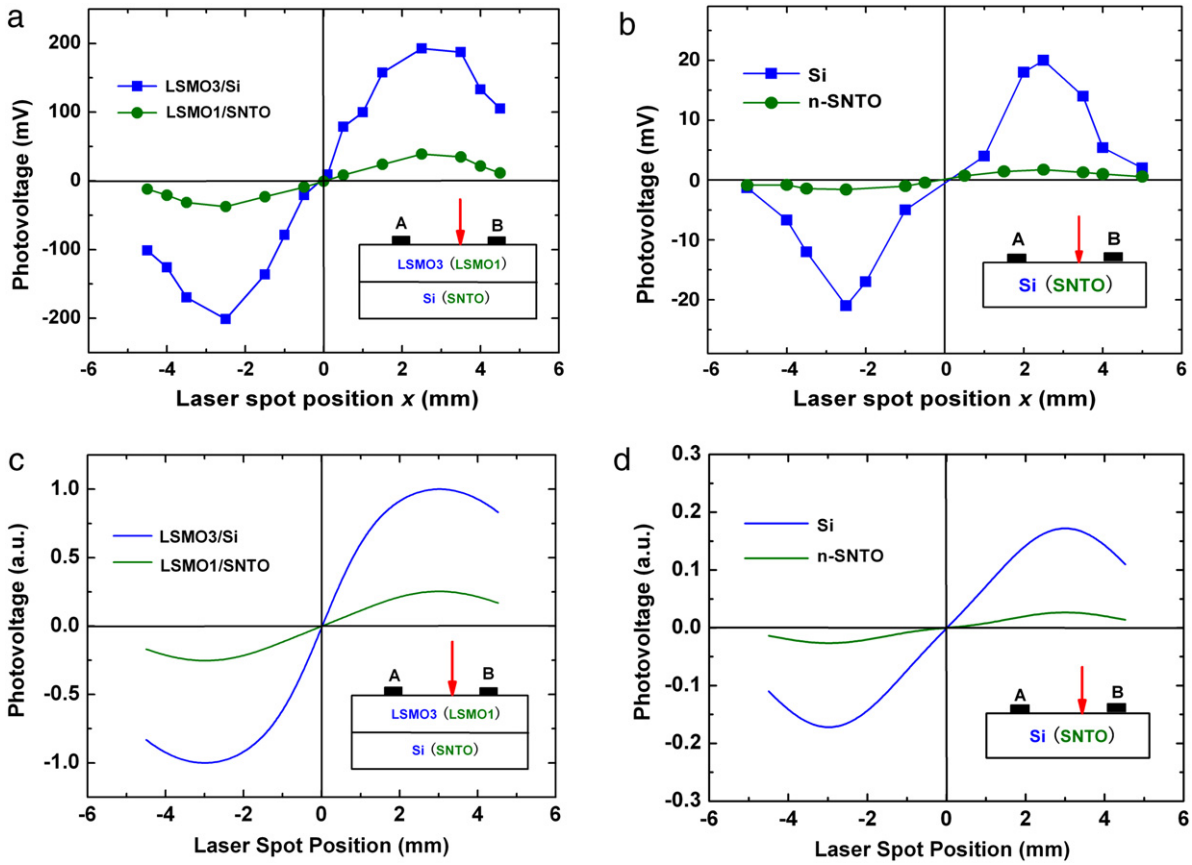

Fig. 1. The experimental (a) and theoretical (c) LPVs of the LSMO side in the LSMO1/SNTO denoted by the green curve and LSMO3/Si denoted by the blue curve; the experimental (b) and theoretical (d) LPVs of SNTO denoted by the green curve and Si denoted by the blue curve. The photovoltage denotes the peak value of LPV between the indium electrodes A ($x = -3$ mm) and B ($x = 3$ mm). The inset shows the schematic setup for LPV measurement. (For interpretation of the references to colour in this figure legend, the reader is referred to the web version of this article.)

enhancement of the LPVs was observed, as compared with those of the substrates.

In order to clarify the underlying mechanisms behind this phenomenon, we carried out self-consistent calculations based on the drift-diffusion model. Some of our early theoretical works confirmed that self-consistent calculations can well describe the transport property of those perovskite oxide heterostructures with weak multi-couplings among the freedoms of the charge, spin, and orbit [12]. Besides, the *time-dependent* two-dimensional drift-diffusion equations [13] can be applied in describing the dynamic process for the movement of photon-induced carriers and the evolution of the electrostatic potential at any location in the complex oxide $p-n$ heterostructures [6], which consist of the Poisson equation and the carrier continuity equations as follows:

$$\frac{\partial^2\phi(x,y,t)}{\partial x^2}+\frac{\partial^2\phi(x,y,t)}{\partial y^2}=-\frac{e}{\varepsilon}[p(x,y,t)-n(x,y,t)+N], \quad (1)$$

$$\frac{\partial p(x,y,t)}{\partial t}=-\frac{1}{e}\nabla\cdot\vec{j}_p(x,y,t)+G(x,y,t)-R(x,y,t), \quad (2)$$

$$\frac{\partial n(x,y,t)}{\partial t}=\frac{1}{e}\nabla\cdot\vec{j}_n(x,y,t)+G(x,y,t)-R(x,y,t), \quad (3)$$

$$\vec{j}_p(x,y,t)=\left[-e\mu_p p(x,y,t)\frac{\partial\phi(x,y,t)}{\partial x}-eD_p\frac{\partial p(x,y,t)}{\partial x}\right]\cdot\boldsymbol{i}_x + \left[-e\mu_p p(x,y,t)\frac{\partial\phi(x,y,t)}{\partial y}-eD_p\frac{\partial p(x,y,t)}{\partial y}\right]\cdot\boldsymbol{i}_y, \quad (4)$$

$$\vec{j}_n(x,y,t)=\left[-e\mu_n n(x,y,t)\frac{\partial\phi(x,y,t)}{\partial x}+eD_n\frac{\partial n(x,y,t)}{\partial x}\right]\cdot\boldsymbol{i}_x + \left[-e\mu_n n(x,y,t)\frac{\partial\phi(x,y,t)}{\partial y}+eD_n\frac{\partial n(x,y,t)}{\partial y}\right]\cdot\boldsymbol{i}_y, \quad (5)$$

where x and y denote the transverse and lateral axes, respectively, $\phi(x,y,t)$ denotes electrostatic potential, $n(x,y,t)$ and $p(x,y,t)$ denote the electron and hole concentrations, respectively, $\vec{j}_n(x,y,t)$ and $\vec{j}_p(x,y,t)$ denote electron and hole current density vectors, respectively, $\boldsymbol{i}_x$ and $\boldsymbol{i}_y$ are the unit vectors along the x and y axes, respectively, e, ε, and N denote the electron charge, the dielectric permittivity, and the net ionized impurity concentrations, respectively, μ_n and μ_p are the mobilities of electrons and holes, respectively, D_n and D_p are the diffusion coefficients of electrons and holes, respectively, k and T denote the Boltzmann constant and the absolute temperature, respectively, $G(x,y,t)$ is the generation rate of the photo-induced electron-hole pairs, which is taken as $G(x,y,t)=I_0(y)\alpha\beta\exp(-\alpha x)$, where α denotes the absorption coefficient, β denotes the quantum efficiency and $I_0(y)$ denotes the incident photon flux density. Moreover, in our calculation, $I_0(y)$ is considered as a Gauss distribution function. $R(x,y,t)$ denotes the Shockley–Read–Hall recombination rate [14]. The lifetimes of electrons and holes are both chosen as 1 ns [12]. Here, D_n and D_p are calculated as $\frac{k_BT}{e}\mu_n$ and $\frac{k_BT}{e}\mu_p$, respectively. At the interface of the heterostructure, the Richardson thermionic emission current [15] is employed as the boundary condition. For simplicity, we did not consider the interfaces of heterostructure/air and heterostructure/contact metal in our model. The initial values of $\phi(x,y,0)$, $n(x,y,0)$ and $p(x,y,0)$ for solving Eqs. (1)–(3) are obtained by solving the nonlinear Poisson equations [13].

By solving the above equations self-consistently, we can obtain the electrostatic potential at any position on the p-type side surface

Table 1
The necessary parameters taken from the reference papers [17,18] or our previous measurements [6,16].

	LSMO1(3)	SNTO	Si
Temperature (K)	300	300	300
Dielectric constant(ε_0)	10.0 [6]	300.0 [6]	11.9 [18]
Electron mobility ($cm^2/(V\,s)$)	10.0 [6]	8.0 [6,17]	1450 [18]
Hole mobility ($cm^2/(V\,s)$)	1.8 [6]	0.1 [6]	500 [18]
Band gap (eV)	0.8 [16]	2.8 [16,17]	1.12 [18]
Net ionized impurity concentrations ($/cm^3$)	4.0×10^{19} (1.0×10^{20}) [6]	1.63×10^{20} [6]	1.0×10^{17}
Photon absorption coefficient (cm^{-1})	1.5×10^5 [17]	1.2×10^5 [17]	4×10^5 [18]

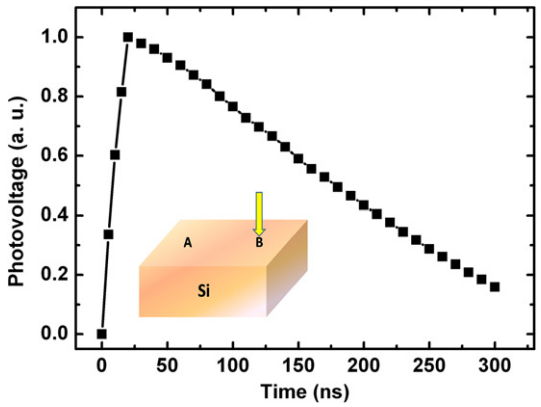

Fig. 2. The calculated curve denotes the dependence of LPV on the time in a single laser pulse, when the contact B is irradiated by the laser. The inset shows the schematic setup.

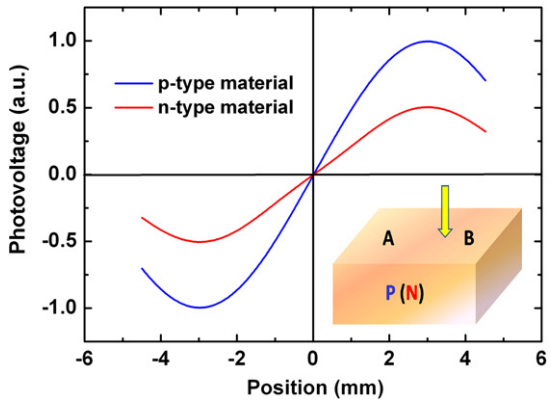

Fig. 3. The calculated LPVs between the electrodes A ($x = -3$ mm) and B ($x = 3$ mm) in the same material with different doping type. The blue and red curves denote the LPVs in the *p*-type and *n*-type Material, respectively. The inset exhibits the schematic setup. (For interpretation of the references to colour in this figure legend, the reader is referred to the web version of this article.)

and *n*-type side surface, respectively. In this way, the dependence of the LPV on the laser spot position can be obtained in the oxide heterostructure we studied. Our calculated results for LPVs on the LSMO side in LSMO1/SNTO and LSMO3/Si heterostructures are shown in Fig. 1(c) as the green curve and blue one, respectively. The calculated LPVs on SNTO and Si substrates are displayed in Fig. 1(d) by the green curve and the blue curve, respectively. The necessary parameters for the calculation are listed in Table 1 [6,16–18]. For simplicity, we use the same parameters for LSMO1 and LSMO3 except the concentration as shown in Table 1. As our model purely describes the charge contribution in the heterostructure and the experimental data includes more complicated factors in the measuring circuit, contacts, and so on, we use a.u. to show our calculated results to compare with the experimental data in the curves. It can be seen that the calculated results are in good agreement with the experimental data. Fig. 2 shows the dependence of LPV on the time in a single laser pulse by our calculation, when the contact B is irradiated by the laser. As the pulse width of laser is 20 ns, the LPV increases rapidly within 20 ns. Then, the LPV decays with time as shown in Fig. 2.

From the present calculation, the mechanisms for the one-order-of-magnitude enhancement of the Dember-effect-induced LPV can be revealed. There are mainly two physical origins. Firstly, we find that the Dember-effect-induced LPV of the *p*-type material is larger than that of the *n*-type material with the same carrier concentration. As illustrated in Fig. 3, we calculated the Dember-effect-induced LPVs of the *p*-type material and *n*-type material with the same carrier concentration of 1×10^{17} cm^{-3}. It can be seen that the LPV of the *p*-type material is almost twice as large as that of the *n*-type material. This can be totally attributed to the difference between the mobilities of electrons and holes. Under the same condition, the amounts of photo-generated electrons and holes are the same in both the *p*-type material and *n*-type material. Consequently, the lateral diffusion current densities, written as $J_{ydif} = eD_n \frac{\partial n}{\partial y} - eD_p \frac{\partial p}{\partial y}$, are the same. However, the main drift carriers for *p*-type material are holes, while the main drift carriers for *n*-type material are electrons. Assuming that the system is in the steady state that the drift current densities can just balance the diffusion current densities, the lateral drift current densities, which is written as $J_{ydrf} = e\mu_n nE_y + e\mu_p pE_y$, are of the same value for the *p*-type material and *n*-type material. Thus, the drift electric field of the *p*-type material should be larger than that of the *n*-type material, as the mobility of holes is smaller than that of electrons. Therefore, it can be concluded that the Dember-effect-induced LPV of the *p*-type material is larger than that of the *n*-type material. Moreover, the Dember-effect-induced THz radiation from the surface of *p*-InAs wafer has been reported as a strong THz emitter [7]. We believe that the present study gives an insight into the physical origin of such an application. Then, we will show why Dember-effect-induced LPV on a heterostructure is much larger than that on a substrate.

Secondly, we find from our calculations that the built-in electric field at the interface between the thin film and the substrate also plays an important role in the LPV effect. To reveal the effect of the built-in electric field, we assumed that the potential difference between the *p*-type region and the *n*-type region was zero and 0.52 V for the structure without and with the built-in electric field in our self-consistent calculations, respectively. Fig. 4 shows the calculated LPVs for the heterostructure with and without the built-in electric field denoted by the blue curve and the red curve, respectively. The upper inset in Fig. 4 indicates the calculated band diagram without the laser illumination. The green arrow pointing from the *n*-type side to the *p*-type side in the upper inset denotes the direction of the built-in field. From Fig. 4, it can be estimated that the heterostructure with a small built-in field of 0.52 V can produce a five times larger LPV than that of the heterostructure without the built-in field. When heterostructures are irradiated by the laser with the photon energy larger than the energy gaps of both the *p*-type side and *n*-type side, electron-hole pairs are produced in these structures. For the structure with the built-in electric field, the photo-generated electron-hole

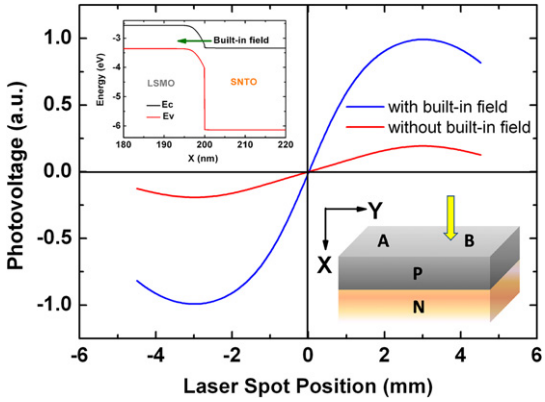

Fig. 4. The blue and red curves denote the calculated LPVs between the electrodes A ($x = -3$ mm) and B ($x = 3$ mm) in the same heterostructures with built-in field and without built-in field, respectively. The lower inset exhibits the schematic setup. The upper inset indicates the calculated band diagram without the laser illumination. The green arrow in the upper inset denotes the direction of the built-in field. (For interpretation of the references to colour in this figure legend, the reader is referred to the web version of this article.)

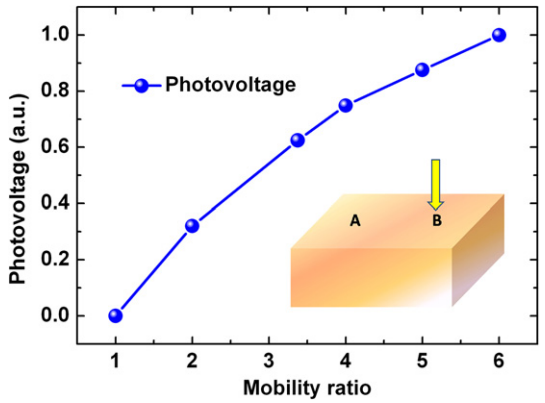

Fig. 5. The curve denotes the dependence of the peak value of LPV on the mobility ratio by our calculation. The inset shows the schematic setup.

pairs can be separated by the built-in electric field. Thereby, the photo-generated holes are swept into the *p*-type layer, and the potential of the irradiation region is raised relative to the situation without the built-in electric field. Hence, the Dember-effect-induced LPV for the structure with the built-in electric field is enhanced compared to the one without the built-in electric field. The combination of the above two mechanisms can well explain the one-order-of-magnitude enhancement of the LPV in the perovskite heterostructures.

In addition, we investigated the dependence of LPV on the mobility ratio. Setting the mobility for holes, we calculated the LPV with various mobility of electrons. The parameters of Si were used in this calculation. As illustrated in Fig. 5, the peak value of the LPV turns to be larger with the increase of mobility ratio between the electron and the hole. Therefore, materials with large mobility ratio can be utilized for the performance improvement of the devices based on the Dember effect.

In conclusion, by solving the *time-dependent* two-dimensional drift-diffusion equations self-consistently, two mechanisms are introduced to explain the greatly enhanced LPV in the perovskite oxide heterostructures, and the theoretical results are in good agreement with the experimental data. We find that the LPV of the *p*-type material is larger than that of the *n*-type material owing to the larger drift electric field induced in the *p*-type material than that in the *n*-type material. Moreover, the LPV can be also enhanced by the built-in field at the interface between the thin film and the substrate. By calculations, we find that the Dember-effect-induced LPV will get larger with the increase of the mobility ratio between the electron and the hole. The understanding of the mechanisms for the enhanced LPV in oxide heterostructures should be useful in further designing of the structures of potential applications in both high-sensitive PSDs and powerful THz sources. Our calculated values are less than half experimental results. We think some unclear mechanisms which we have not included in our model may also play some role in the LPV measurements. Therefore, further investigation even in the theoretical aspect is still ongoing.

Acknowledgements

This work has been supported by the National Natural Science Foundation of China and the National Basic Research Program of China.

References

[1] W. Schottky, Phys. Z 31 (1930) 913.
[2] J.T. Wallmark, Proc. IRE 45 (1957) 474.
[3] J. Henry, J. Livingstone, Adv. Mater. 13 (2001) 1022;
J. Henry, J. Livingstone, J. Phys. D: Appl. Phys. 41 (2008) 165106.
[4] K.J. Jin, H.B. Lu, K. Zhao, C. Ge, M. He, G.Z. Yang, Adv. Mater. 21 (2009) 4636.
[5] K.J. Jin, K. Zhao, H.B. Lu, L. Liao, G.Z. Yang, Appl. Phys. Lett. 91 (2007) 081906.
[6] L. Liao, K.J. Jin, C. Ge, C.L. Hu, H.B. Lu, G.Z. Yang, Appl. Phys. Lett. 96 (2010) 062116.
[7] M. Tonouchi, Nat. Photonics 1 (2007) 97;
K. Liu, J.Z. Xu, T. Yuan, X.-C. Zhang, Phys. Rev. B 73 (2006) 155330.
[8] P. Gu, M. Tani, S. Kono, K. Sakai, X.-C. Zhang, J. Appl. Phys. 91 (2002) 5533.
[9] T. Dekorsy, H. Auer, H.J. Bakker, H.G. Roskos, H. Kurz, Phys. Rev. B 53 (1996) 4005.
[10] T. Dekorsy, T. Pfeifer, W Kütt, H. Kurz, Phys. Rev. B 47 (1993) 3842.
[11] H.B. Lu, K.-J. Jin, Y.H. Huang, M. He, K. Zhao, B.L. Cheng, Z.H. Chen, Y.L. Zhou, S.Y. Dai, G.Z. Yang, Appl. Phys. Lett. 86 (2005) 241915;
G.Z. Yang, H.B. Lu, F. Chen, T. Zhao, Z.H. Chen, J. Cryst. Growth 227–228 (2001) 929.
[12] Q.L. Zhou, K.J. Jin, H.B. Lu, P. Han, Z.H. Chen, K. Zhao, Y.L. Zhou, G.Z. Yang, Europhys. Lett. 71 (2005) 283;
C.L. Hu, K.J. Jin, P. Han, H.B. Lu, L. Liao, G.Z. Yang, Solid State Commun. 149 (2009) 334;
C.L. Hu, K.J. Jin, P. Han, H.B. Lu, L. Liao, G.Z. Yang, Appl. Phys. Lett. 93 (2008) 162106.
[13] Siegfried Selberherr, Analysis and Simulation of Semiconductor Devices, Springer, New York, 1984.
[14] W. Shockley, W.T. Read, Phys. Rev. 87 (1952) 835.
[15] K. Yang, J.R. East, G.I. Haddad, Solid State Electron. 36 (1993) 321.
[16] P. Han, K.J. Jin, H.B. Lu, Q.L. Zhou, Y.L. Zhou, G.Z. Yang, Appl. Phys. Lett. 91 (2007) 182102;
K.J. Jin, H.B. Lu, Q.L. Zhou, K. Zhao, B.L. Cheng, Z.H. Chen, Y.L. Zhou, G.Z. Yang, Phys. Rev. B 71 (2005) 184428.
[17] S. Myhajlenko, A. Bell, F. Ponce, J.L. Edward Jr., Y. Wei, B. Craigo, D. Convey, H. Li, R. Liu, J. Kulik, J. Appl. Phys. 97 (2004) 014101;
R. Moos, K.H. Härdtl, J. Appl. Phys. 80 (1996) 393;
S. Chambers, Y. Liang, Z. Yu, R. Droopad, J. Ramdani, K. Eisenbeiser, Appl. Phys. Lett. 77 (2000) 1662;
M.W. Kim, P. Murugavel, S. Parashar, J.S. Lee, T.W. Noh, New J. Phys. 6 (2004) 156;
M.I. Cohen, R.F. Blunt, Phys. Rev. 168 (1968) 929.
[18] K.W. Böer, Survey of Semiconductor Physics Volume II, Van Nostrand Reinhold, New York, 1990;
G.E. Jellison Jr., F.A. Modine, J. Appl. Phys. 53 (1982) 3745.